nature photonics

ARTICLES

PUBLISHED ONLINE: 26 APRIL 2009 | DOI: 10.1038/NPHOTON.2009.69

Bulk heterojunction solar cells with internal quantum efficiency approaching 100%

Sung Heum Park[1,2], Anshuman Roy[1], Serge Beaupré[3], Shinuk Cho[1,2], Nelson Coates[1], Ji Sun Moon[1,2], Daniel Moses[1], Mario Leclerc[3], Kwanghee Lee[1,2]* and Alan J. Heeger[1,2]*

We report the fabrication and measurement of solar cells with 6% power conversion efficiency using the alternating co-polymer, poly[*N*-9′′-hepta-decanyl-2,7-carbazole-alt-5,5-(4′,7′-di-2-thienyl-2′,1′,3′-benzothiadiazole) (PCDTBT) in bulk heterojunction composites with the fullerene derivative [6,6]-phenyl C_{70}-butyric acid methyl ester ($PC_{70}BM$). The PCDTBT/$PC_{70}BM$ solar cells exhibit the best performance of any bulk heterojunction system studied to date, with $J_{SC} = 10.6$ mA cm^{-2}, $V_{OC} = 0.88$ V, $FF = 0.66$ and $\eta_e = 6.1\%$ under air mass 1.5 global (AM 1.5 G) irradiation of 100 mW cm^{-2}. The internal quantum efficiency is close to 100%, implying that essentially every absorbed photon results in a separated pair of charge carriers and that all photogenerated carriers are collected at the electrodes.

Polymer bulk heterojunction (BHJ) solar cells based on composites of an electron-donating conjugated polymer and an electron-accepting fullerene offer promise for the realization of a low-cost, printable, portable and flexible renewable energy source[1–4]. Although BHJ solar cell performance has steadily improved, with power conversion efficiencies (PCE $\equiv \eta_e$) approaching 5%, further improvements in efficiency are required for large-scale commercialization[5–7].

Rather than using a single junction architecture, the fundamental BHJ concept involves the self-assembly of nanoscale heterojunctions by spontaneous phase separation of the donor (polymer) and the acceptor (fullerene). As a result of this spontaneous phase separation, charge-separating heterojunctions are formed throughout the bulk of the material[2].

Over the past decade, research has focused on regio-regular poly(3-hexylthiophene) (P3HT) as the standard electron-donating material in polymer BHJ solar cells, with important progress having been made in understanding the device science and the associated improvements in device efficiency. Relatively high-performance polymer BHJ solar cells made from a mixture of P3HT and [6,6]-phenyl C61 butyric acid methyl ester (PCBM) have been reported, with maximum PCEs of $\eta_e = 4$–5% (refs 5–7). Although approaches to improving the efficiency of P3HT/PCBM cells are still being reported, the relatively large bandgap of P3HT (∼1.9 eV) limits the fraction of the solar spectrum that can be harvested, and the relatively small energy difference between the top of the π-band (highest occupied molecular orbital, HOMO) of P3HT and the lowest unoccupied molecular orbital (LUMO) of the fullerene acceptor results in a low open-circuit voltage, $V_{OC} \approx 0.6$ V. These fundamental energies defined by the electronic structure of the semiconducting polymer (the energy gap and the HOMO energy) must be decreased in order achieve polymer BHJ solar cells with PCEs of 6% and higher.

Recently, several classes of low-bandgap polymers have been developed to better harvest the solar spectrum with deeper HOMO energies that can potentially increase V_{OC} (refs 8–12). These polymers are designed to make use of internal charge transfer from an electron-rich unit to an electron-deficient moiety within the fundamental repeat unit. Among them, alternating co-polymers based on poly(2,7-carbazole) derivatives[11,12], with a suite of electron-deficient moieties to choose from, are particularly interesting (see Fig. 1). The different electron-deficient moieties can be used to tune the electronic energy gap of the semiconducting polymer, while the deep HOMO of the carbazole leads to higher values for V_{OC} (ref. 11). The implied flexibility in the synthesis can lead to both a smaller bandgap that enables the harvesting of a larger fraction of the solar radiation spectrum, and a deeper HOMO energy that increases the open circuit voltage of the photovoltaic device. In their initial report of the synthesis and device performance of PCDTBT, Leclerc and colleagues demonstrated a PCE of 3.6% from a BHJ cell with V_{OC} value approaching 0.9 V (ref. 12).

We report here solar cells with 6% PCE from BHJ composites comprising PCDTBT/[6,6]-phenyl C71 butyric acid methyl ester ($PC_{70}BM$) with short-circuit current $J_{SC} = 10.6$ mA cm^{-2}, open circuit voltage $V_{OC} = 0.88$ V and fill factor $FF = 0.66$ under air mass 1.5 global (AM 1.5 G) irradiation of 100 mW cm^{-2}. The internal quantum efficiency (IQE) is close to 100%, implying that essentially every absorbed photon results in a separated pair of charge carriers and that all photogenerated carriers are collected at the electrodes.

Titanium oxide optical spacer and hole blocking layer

Historically, a relatively low PCE has been demonstrated in polymer solar cells made from polymers that make use of the internal charge transfer concept, including PCDTBT[11,12]. This low PCE has been limited by the relatively low photocurrent obtained from these devices. In BHJ cells, the photocurrent generation is governed by two main factors[13,14]: (i) the fractional number of absorbed photons in the active layer (relative to the total flux of photons from the solar spectrum) and (ii) the IQE defined by the fraction of collected carriers per absorbed photon. In principle, one can simply increase the thickness of the active layer to absorb more light. However, because of the relatively low carrier mobility of the disordered materials (cast from solution with subsequent phase separation), increasing the thickness increases the internal resistance of the device. Consequently, the fill factor typically

[1]Center for Polymers and Organic Solids, University of California at Santa Barbara, Santa Barbara, California 93106, USA, [2]Heeger Center for Advanced Materials, Gwangju Institute of Science and Technology, Gwangju 500-712, South Korea, [3]Department of Chemistry, University of Laval, G1K 7P4 Quebec City, Quebec, Canada. *e-mail: klee@gist.ac.kr; ajhe@physics.ucsb.edu

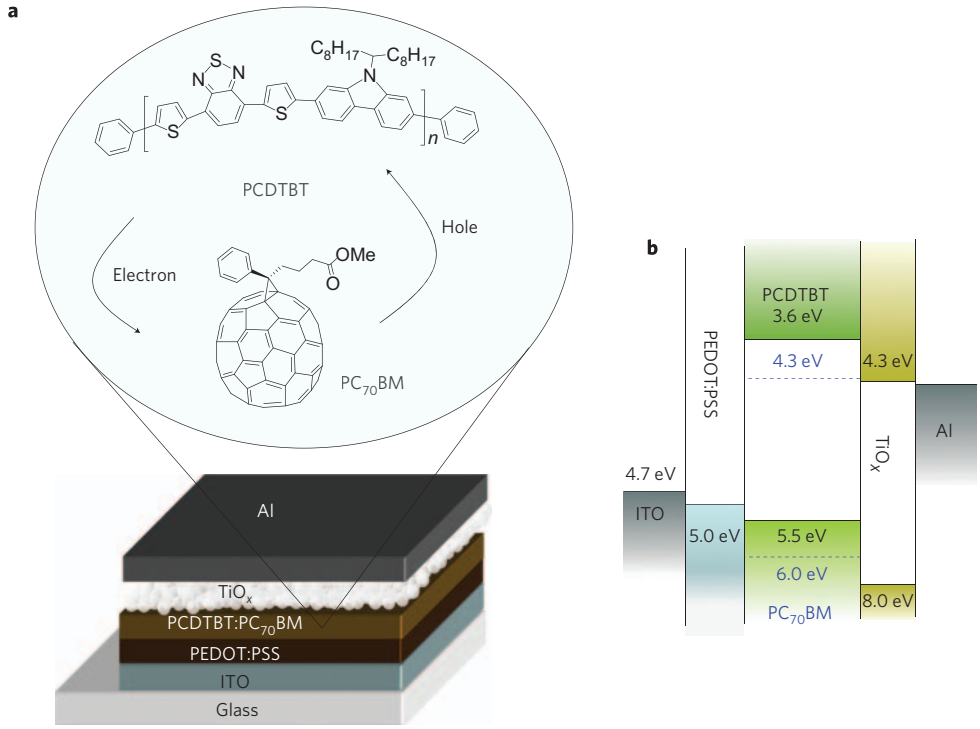

Figure 1 | Device structure and energy level diagram of the components. a, The bulk heterojunction (BHJ) film is a phase separated blend of PCDTBT and $PC_{70}BM$. The inset shows the transfer of photogenerated electrons from PCDTBT to $PC_{70}BM$. The titanium oxide (TiO_x) layer is introduced as an optical spacer on top of the BHJ layer. **b**, Energy level diagram of the components of the device.

plummets as the thickness is increased. Based on this simple analysis, we consider the following approach towards obtaining higher photocurrent: maximizing the photon absorption for a fixed active layer thickness while simultaneously improving the IQE.

To increase the photocurrent while keeping the thickness fixed, we used an optical spacer between the photo-active layer and the top electrode; because of the optical spacer, the maximum light intensity is redistributed to be within the active charge separating BHJ layer. The utility of the optical spacer has been reproduced in recent publications[15]. In parallel, by choosing optimal conditions for processing, we have demonstrated a nanoscale BHJ morphology that results in nearly 100% IQE. This dual focused approach applied to PCDTBT/$PC_{70}BM$ results in PCE, $n_e \geq 6\%$; the highest value reported to date for polymer BHJ solar cells.

Figure 1 shows the structure of the BHJ device together with the molecular structures and an energy level diagram of the component materials. From the fundamental physics of the open-circuit voltage associated with the donor–acceptor heterojunction and the empirical relationship demonstrated in refs 16–18, the relatively deep HOMO energy of PCDTBT, ~5.5 eV, should result in a higher open-circuit voltage. Moreover, because the spherical symmetry of the fullerene has been lifted in $PC_{70}BM$ (compared to PCBM), the PCDTBT/$PC_{70}BM$ BHJ material has higher absorption and, consequently, enhanced photocurrent[19,20].

The solution processible titanium sub-oxide (TiO_x) layer[15,21,22] was introduced as an optical spacer[21] and as a hole blocker[23] (see Supplementary Information) between the BHJ layer and the top metal electrode. The TiO_x layer redistributes the light intensity within the BHJ by changing the optical interference between the incident light and the light reflected from the metal electrode[24,25]. As the active layer thickness decreases, the intensity of reflected light increases, and the optical interference effect becomes more pronounced. Hence, we expect that the efficacy of the TiO_x layer will be higher for thinner active layers. Hole blocking by the TiO_x is also more important for thinner-film devices. In the PCDTBT:$PC_{70}BM$ solar cells reported here, the thickness of the active layer is ~80 nm, and the TiO_x layer thickness is ~10 nm. With this configuration, we are able to make good use of the optical spacer by avoiding destructive interference within the charge separating layer between the incident light and the light reflected from the aluminium–TiO_x interface. In addition, the bottom of the conduction band of TiO_x matches the LUMO of $PC_{70}BM$. Finally, the relatively high electron mobility of $PC_{70}BM$ and the hole-blocking feature of TiO_x enable efficient electron collection without a significant increase in the series resistance[21–23].

Figure 2a shows the absorption spectra of PCDTBT solar cells with and without the TiO_x layer. The total absorption by the active layer (including the doubled path length in the BHJ layer as a result of reflection from the aluminium electrode) was measured in reflection geometry as illustrated in the inset of Fig. 2a. Comparing two devices with the same active layer thickness (80 nm), a substantial enhancement in absorption is observed in the device with the TiO_x layer. Consequently, as shown in Fig. 2b, the device with the TiO_x layer demonstrates higher IPCE (incident photon-to-current efficiency) throughout the visible range compared with the device without the TiO_x layer. Because the integration of the product of the IPCE with the AM 1.5 solar spectrum is equal to the short-circuit current, the higher short-circuit current (see Fig. 2c) of the device with TiO_x is consistent with the higher IPCE values.

Nanoscale morphology and photocurrent generation

Note, however, that the photocurrent is determined by the product of the total number of absorbed photons within the solar spectrum and the IQE of the device[26–28]. The IQE is determined by a three-step process[26–28]: (i) migration/diffusion of the photogenerated excitations to the PCDTBT/$PC_{70}BM$ interface; (ii) exciton dissociation and charge separation at the interface; and (iii) collection of charge carriers at the ITO and aluminium electrodes. Because of step (i), the nanoscale phase separation in BHJ materials must be less than 20 nm because the exciton diffusion length is generally less than

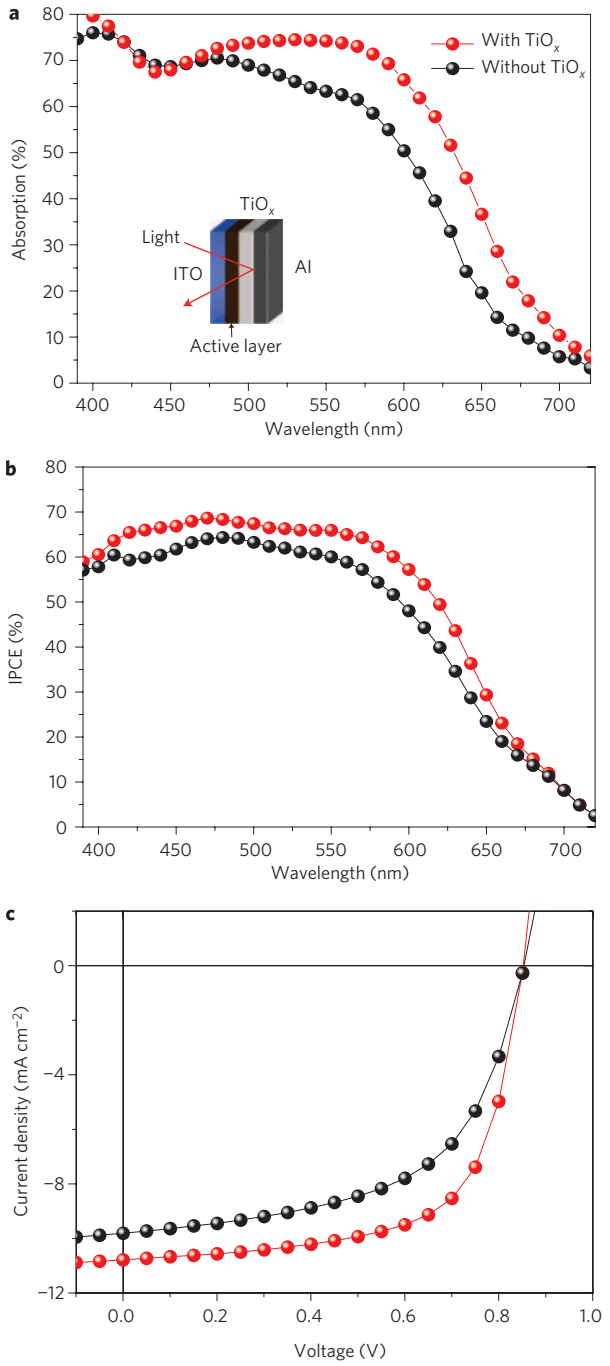

Figure 2 | The effects of TiO_x layer as an optical spacer on device performance. a, Total absorption in the active layer measured in a reflection geometry with the TiO_x layer (red symbols) and without the TiO_x layer (black symbols). The inset shows a schematic of the device structure. **b**, Incident photon-to-current efficiency (IPCE) spectra with the TiO_x layer (red symbols) and without the TiO_x layer (black symbols). **c**, Current density versus voltage characteristics (*J*–*V*) of the device with the TiO_x layer (red symbols) and without the TiO_x layer (black symbols).

10 nm (refs 29,30). In addition, smaller-scale phase separation creates larger-area PCDTBT:$PC_{70}BM$ interfaces where charge separation can take place. For step (ii), a sufficiently large energy difference between the PCDTBT LUMO and the $PC_{70}BM$ LUMO is required for ultrafast photoinduced electron transfer. For step (iii), both the PCDTBT and $PC_{70}BM$ phases must form percolated networks with few charge-trapping sites or 'dead ends'. The ultrafast photo-induced charge transfer (<100 fs) at the polymer–fullerene interface ensures that the charge separation efficiency approaches 100% (refs 2,31,32). Hence, the molecular organization and morphology on the nanometre scale as described by steps (i) and (ii), and the nanoscale morphology and the interface between the cathode and the TiO_x/BHJ as described in step (iii), provide the route to high IQE.

The nanoscale morphology of the PCDTBT:$PC_{70}BM$ BHJ is strongly affected by processing parameters such as choice of solvents, blend ratio of PCDTBT to $PC_{70}BM$, solution concentration, thermal annealing, and the molecular structure of the component materials[33–35]. In our experiments, thermal annealing of the PCDTBT:$PC_{70}BM$ system at high temperatures reduced the *FF*, J_{SC} and V_{OC} (see Supplementary Information). Thus, the use of thermal annealing is eliminated as a strategy for improving device performance. However, it is well known that for polymer-based solar cells, performance is strongly affected by both the solvent and the blend ratio[33–36]. This is expected because the solvent is known to affect the BHJ domain size, and the donor/acceptor blend ratio determines the formation of percolated networks.

Figure 3a–c shows defocused[37,38] transmission electron microscope (TEM) images of PCDTBT:$PC_{70}BM$ (1:4 ratio) films dissolved in chloroform (CF), chlorobenzene (CB) and dichlorobenzene (DCB), respectively. Although large dark clusters (200 and 300 nm) are observed in the CF and CB films, clearly defined nanoscale phase separation is observed in the film cast from DCB. These features are also observed in the surface phase images measured by atomic force microscopy (AFM), as shown in the insets of the TEM images. The higher electron density of $PC_{70}BM$ compared with PCDTBT causes electrons to be scattered more efficiently by the $PC_{70}BM$ from the TEM beam. Thus, the darker regions in the TEM images are regions of phase-separated $PC_{70}BM$. Because the exciton diffusion length (<10 nm) is much smaller than the 200–300 nm features seen in Fig. 3a,b, photo-generated excitons will often recombine before reaching the interfaces in films cast from solution in CB or CF, causing reduced charge carrier generation at the interfaces and a concomitant loss of photocurrent.

Figure 3d shows the IPCE spectra of solar cells comprising BHJ films cast from CF, CB, DCB and from a mixture of CB and DCB. The cell fabricated with a BHJ film cast from DCB has a higher IPCE over the entire excitation spectrum compared to devices comprising films cast from either CF or CB. Processing from a mixture of DCB and CB also increases the IPCE compared to processing from pure CB. Increasing the amount of DCB in the CB/DCB mixture increases the contribution from $PC_{70}BM$ to the IPCE, as is evident from the pronounced peaks around 400 and 450 nm.

Figure 3a–c demonstrates that DCB results in significantly smaller nanoscale phase separation. Therefore, the increased IPCE shown in Fig. 3d and obtained from devices made with films cast from pure DCB or from mixtures of CB and DCB results from the nanoscale phase separation. The enhanced J_{SC} and higher *FF* (see Fig. 3e) imply the formation of well-connected percolated networks for each of the phase-separated components (donor and acceptor). Thus, using DCB evidently also leads to better-connected percolated networks, which, in combination with the nanoscale phase separation, improve the device performance.

Obviously, the connectivity is sensitive to the blend ratio of PCDTBT to $PC_{70}BM$. Figure 4a–d shows TEM images of PCDTBT:$PC_{70}BM$ films cast from DCB with increasing amounts of $PC_{70}BM$. As the amount of $PC_{70}BM$ progressively increases, the nanoscale phase separation can be seen more clearly, with gradual emergence of a 'fibrillar' PCDTBT nanostructure. This fibrillar PCDTBT nanostructure is most pronounced in films at the 1:4 blend ratio, implying that increasing the amount of $PC_{70}BM$ causes the PCDTBT network to form longer and better connected pathways.

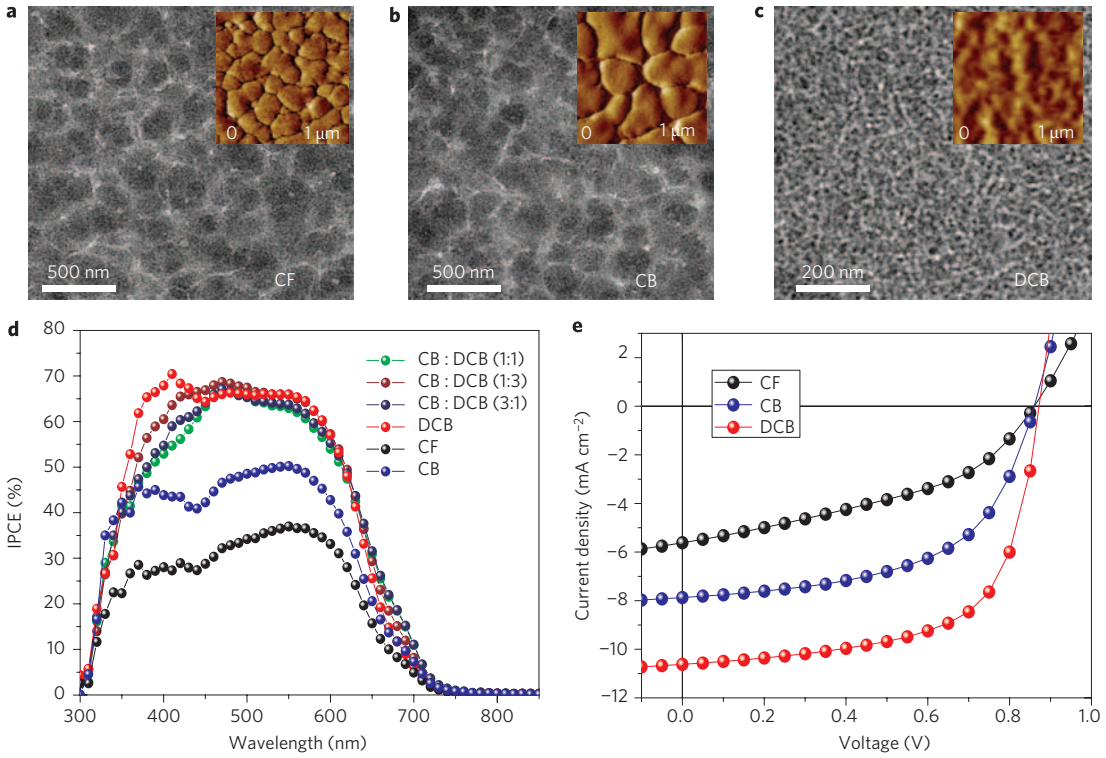

Figure 3 | The effects of CF, CB and DCB solvents on film morphology and device performance. a–c, TEM images of PCDTBT:$PC_{70}BM$ films spin-cast from CF (**a**), CB (**b**) and DCB (**c**) solvents. The insets show the surface phase images measured by atomic force microscopy (AFM). **d**,**e**, IPCE spectra (**d**) and *J–V* characteristics (**e**) of the devices fabricated with films cast from CF, CB and DCB.

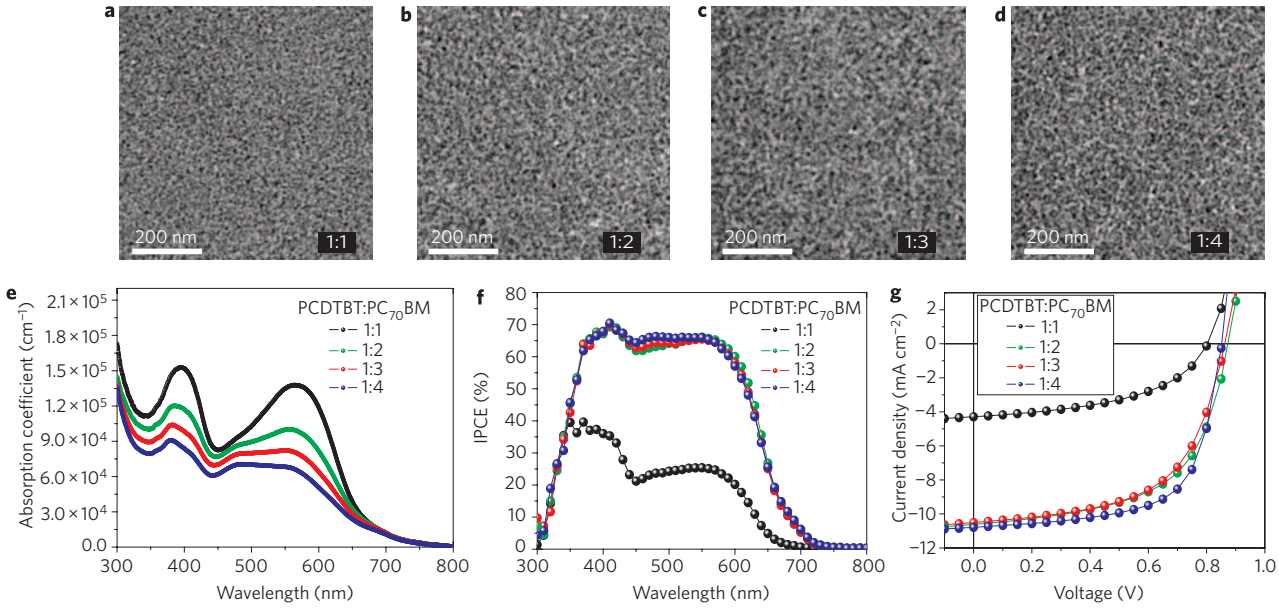

Figure 4 | The effect of blending ratio on film morphology and device performance. a–d, TEM images of the PCDTBT:$PC_{70}BM$ blend films spin-cast from DCB with increasing amounts of $PC_{70}BM$: blending ratios 1:1 (**a**), 1:2 (**b**), 1:3 (**c**) and 1:4 (**d**). **e**, Absorption coefficients of the films with blend ratios of 1:1, 1:2, 1:3 and 1:4. **f**, IPCE spectra for the same films as in **e. g**, *J–V* characteristics of the devices fabricated using BHJ films with blend ratios of 1:1, 1:2, 1:3 and 1:4.

Internal quantum efficiency

The morphology observed in Fig. 4d, using the 1:4 ratio of PCDTBT to $PC_{70}BM$, is ideal for polymer solar cell performance, as is made evident by the increased IQE. However, 80% of the film in terms of mass is now made of $PC_{70}BM$, which has only weak absorption in the visible spectral range. This is evident from the plot of the absorption coefficient shown in Fig. 4e. The decreased absorption coefficient for the 1:4 film reduces the number of absorbed photons in the active layer for fixed film thickness.

To determine the optimum blend ratio, we used the IPCE and *J–V* characteristics of the solar cells. Figure 4f shows the IPCE spectra of solar cells with various blend ratios. Although the IPCE curve obtained from the 1:1 device shows a poor photo-response,

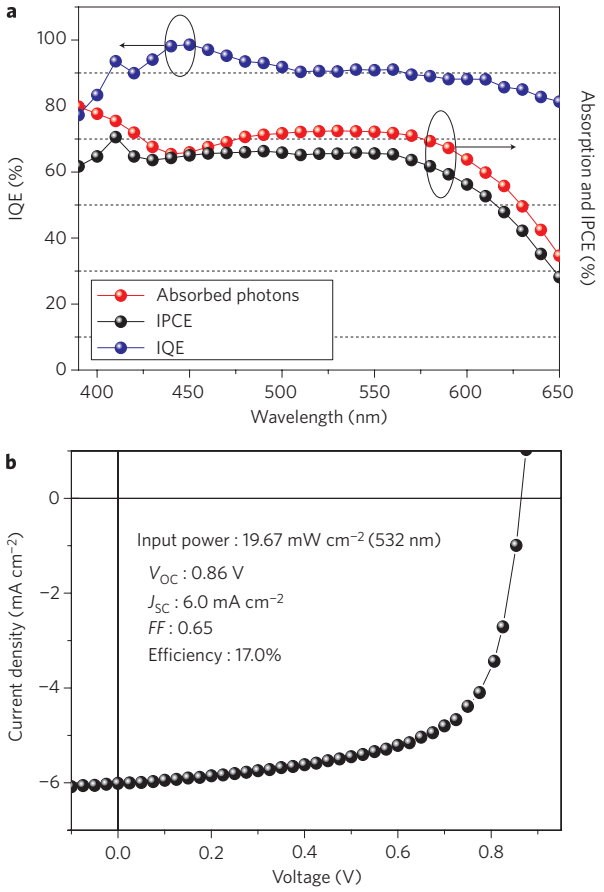

Figure 5 | Internal quantum efficiency (IQE) of PCDTBT:PC$_{70}$BM solar cells. a, IQE values of the 1:4 device with film cast from DCB. The red line shows the total absorption of the device, and the black line the IPCE. **b**, *J–V* characteristics of the device under monochromatic 532-nm light.

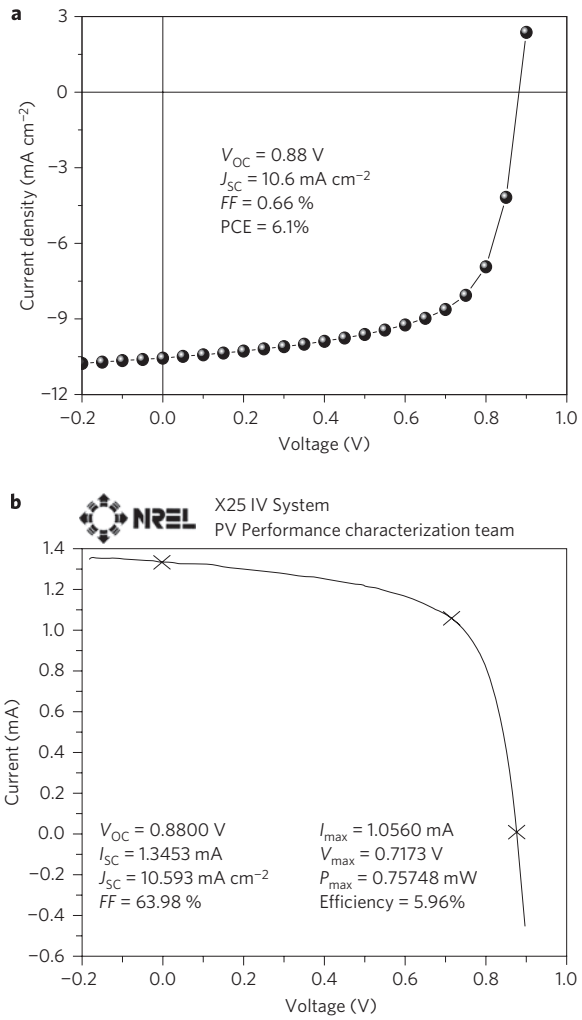

Figure 6 | Power conversion efficiency of PCDTBT:PC$_{70}$BM solar cells. a, *J–V* characteristics of a PCDTBT:PC$_{70}$BM solar cell under AM 1.5 G irradiation with an intensity of 100 mW cm^{-2}. **b**, NREL-certified *J–V* characteristics of a PCDTBT:PC$_{70}$BM solar cell.

comparable (and better) IPCE values are obtained from the 1:2, 1:3 and 1:4 ratios in the BHJ films. This observation is in good agreement with the *J–V* characteristics shown in Fig. 4 g. However, the *FF* values vary significantly amongst devices made from BHJ films with different blend ratios; the *FF* progressively increases as the PCDTBT to PC$_{70}$BM ratio decreases from 1:2 to 1:4. The photogenerated mobile carriers must be transported by means of percolated pathways to the respective electrodes. Breaks and 'dead ends' in the percolation pathways of the 1:1, 1:2 and 1:3 devices as seen in Fig. 4a–c increase the series resistance, and decrease the *FF*.

Measurements of the total absorption spectrum and the IPCE of the PCDTBT/PC$_{70}$BM solar cells enabled the calculation of the IQE spectrum[24,25,28] shown in Fig. 5a, where the red line indicates the total absorption of the 1:4 device and the black line the IPCE spectrum. We find that the PCDTBT/PC$_{70}$BM solar cells have remarkably high IQE values (that is, high efficiency of collected carriers per incident absorbed photon). The IQE (blue line) of the PCDTBT/PC$_{70}$BM solar cells approaches 100% around 450 nm and stays near or even above 90% throughout the entire absorption spectrum (400–650 nm). Such a high IQE is remarkable, indicating that nearly every absorbed photon leads to a separated pair of charge carriers and that all photogenerated carriers are collected at the electrodes.

Solar cell efficiency under monochromatic green light

The high efficiency of the PCDTBT/PC$_{70}$BM solar cells is further demonstrated when irradiated with monochromatic light. Figure 5b shows the *J–V* characteristics of a PCDTBT/PC$_{70}$BM BHJ device under monochromatic irradiation (532 nm) with an intensity of 19.67 mW cm^{-2}. The power conversion efficiency is $\eta_e = 17\%$ with $FF = 65\%$, $V_{OC} = 0.86$ V and $J_{SC} = 6.0$ mA cm^{-2}. Note that the measured 17% efficiency is consistent with IQE $\approx$ 95% at 532 nm when calculated directly from the *J–V* curve and the relatively low optical density at 532 nm (at 532 nm ~30% of the incident light is reflected out through the front surface). Because the IPCE of the device is nearly constant throughout the entire absorption spectrum (400–650 nm), it is possible to get ~17% efficiency from the entire absorption spectrum of PCDTBT. Therefore, the observation of $\eta_e = 17\%$ at 532 nm demonstrates that efficiencies of 10–15% should be achievable with BHJ cells fabricated using semiconducting polycarbazole derivatives with absorption spectra that extend deeper into the infrared; that is, with smaller energy gaps and similarly high IPCE. Tandem cells offer the promise of significantly higher values[4].

Power conversion efficiency of 6% under AM 1.5 G irradiation

Under standard measurement conditions[39,40], the PCDTBT/PC$_{70}$BM solar cells exhibit high PCE. The *J–V* characteristics of the device under AM 1.5 G irradiation from a calibrated solar simulator with irradiation intensity of 100 mW cm^{-2} are shown in Fig. 6a. The PCDTBT/PC$_{70}$BM solar cells reproducibly yield $J_{SC} = 10.6$ mA cm^{-2}, $V_{OC} = 0.88$ V, $FF = 0.66$ and $\eta_e = 6.1\%$. More than 20 out of 100 devices demonstrated efficiencies greater

than 6%. The highest value that we obtained in our laboratory was 6.2% with no antireflective coating on the glass. One of the PCDTBT/$PC_{70}BM$ solar cells with an initial efficiency of 6.1% (without antireflective coating) was sent to NREL for certification, after monitoring and ensuring the device performance for one week. NREL returned the device with a certified efficiency of 5.96%, as shown in Fig. 6b. Given the significant time lag between our sending the device to NREL and the measurement at NREL, we naturally expect some degradation. In fact, lifetime data gathered in our laboratory show that the device had already degraded somewhat by the time the NREL measurement was performed (see Supplementary Information).

Conclusion

In conclusion, we have successfully demonstrated high-efficiency BHJ solar cells comprising PCDTBT and $PC_{70}BM$ (1:4 ratio) as the active charge separating layer. With PCDTBT/$PC_{70}BM$, neither thermal annealing[6,36] nor the addition of processing additives[9,41] are required for achieving high efficiency. The PCDTBT/$PC_{70}BM$ solar cells exhibit $\eta_e = 6\%$ under AM 1.5 irradiation, the highest certified value reported to date. More important, the IQE of the PCDTB/$PC_{70}BM$ solar cells approaches 100%, implying that every photon absorbed leads to a separated pair of charge carriers and that every photogenerated mobile carrier is collected at the electrodes.

Methods

Device fabrication. Solar cells were fabricated on an indium tin oxide (ITO)-coated glass substrate with the following structure: ITO-coated glass substrate/poly(3,4-ethylenedioxythiophene) (PEDOT:PSS)/PCDTBT:$PC_{70}BM$/TiO_x/Al. The ITO-coated glass substrate was first cleaned with detergent, ultrasonicated in acetone and isopropyl alcohol, and subsequently dried overnight in an oven. PEDOT:PSS (Baytron PH) was spin-cast from aqueous solution to form a film of 40 nm thickness. The substrate was dried for 10 min at 140 °C in air and then transferred into a glove box to spin-cast the charge separation layer. A solution containing a mixture of PCDTBT:$PC_{70}BM$ (1:4) in dichlorobenzene solvent with a concentration of 7 mg/ml was then spin-cast on top of the PEDOT/PSS layer. The film was dried for 60 min at 70 °C in the glove box. The TiO_x precursor solution diluted 1:200 in methanol was spin-cast in air on top of the PCDTBT:$PC_{70}BM$ layer (5,000 rpm for 40 s). The sample was heated at 80 °C for 10 min in air. Then, an aluminium (Al, 100 nm) electrode was deposited by thermal evaporation in a vacuum of about 5×10^{-7} torr. Current density–voltage (J–V) characteristics of the devices were measured using a Keithley 236 Source Measure Unit. Solar cell performance used an Air Mass 1.5 Global (AM 1.5 G) solar simulator with an irradiation intensity of 1,000 W m^{-2}. An aperture (12.7 mm^2) was used on top of the cell to eliminate extrinsic effects such as crosstalk, waveguiding, shadow effects and so on. The spectral mismatch factor was calculated by comparison of the solar simulator spectrum and the AM 1.5 spectrum at room temperature.

Measurement system. Our measurement system yielded data in precise agreement with measurements made at NREL. Results for cells returned to us after NREL measurement had expected values. Our integrated IPCE values always agreed with the measured short-circuit current to within a few percent.

TEM microscopy. Specimens were prepared by first casting a PCDTBT:$PC_{70}BM$ blend thin film on glass. The films were baked at 70 °C for 1 h, and then removed from the nitrogen environment and scored with a diamond scribe to define the sample size. The substrate and film were immersed in deionized water for 20 min and sonicated to promote delamination. Resulting pieces of the film were transferred to a PELCO copper TEM grid with a carbon/Formvar support grid. TEM specimens were allowed to dry under low heat to remove excess water from the transfer process. Light field imaging was performed in an FEI T20 TEM using proper defocus for additional phase contrast from the relatively amorphous polymer material.

Received 19 December 2008; accepted 24 March 2009; published online 26 April 2009

References

1. Sariciftci, N. S., Smilowitz, L., Heeger, A. J. & Wudl, F. Photoinduced electron transfer from a conducting polymer to buckminsterfullerene. *Science* **258,** 1474–1476 (1992).
2. Yu, G., Gao, J., Hemmelen, J. C., Wudl, F. & Heeger, A. J. Polymer photovoltaic cells: enhanced efficiencies via a network of internal donor–acceptor heterojunctions. *Science* **270,** 1789–1791 (1995).
3. Halls, J. J. *et al.* Efficient photodiodes from interpenetrating polymer networks. *Nature* **376,** 498–500 (1995).
4. Kim, J. *et al.* Efficient tandem polymer solar cells fabricated by all-solution processing. *Science* **317,** 222–225 (2007).
5. Li, G. *et al.* High-efficiency solution processible polymer photovoltaic cells by self-organization of polymer blends. *Nature Mater.* **4,** 864–868 (2005).
6. Ma, W. Yang, C., Gong, X., Lee, K. & Heeger, A. J. Thermally stable, efficient polymer solar cells with nanoscale control of the interpenetrating network morphology. *Adv. Funct. Mater.* **15,** 1617–1622 (2005).
7. Kim, Y. *et al.* A strong regioregularity effect in self-organizing conjugated polymer films and high-efficiency polythiophene:fullerene solar cells. *Nature Mater.* **5,** 197–203 (2006).
8. Muhlbacher, D. *et al.* High photovoltaic performance of a low-bandgap polymer. *Adv. Mater.* **18,** 2884–2889 (2006).
9. Peet, J. *et al.* Efficiency enhancement in low-bandgap polymer solar cells by processing with alkane dithiols. *Nature Mater.* **6,** 497–500 (2007).
10. Wang, E. *et al.* High-performance polymer heterojunction solar cells of a polysilafluorene derivative. *Appl. Phys. Lett.* **92,** 033307–033310 (2008).
11. Blouin, N. *et al.* Toward a rational design of poly(2,7-carbazole) derivatives for solar cells. *J. Am. Chem. Soc.* **130,** 732–742 (2008).
12. Blouin, N., Michaud, A. & Leclerc, M. A low-bandgap poly(2,7-carbazole) derivative for use in high-performance solar cells. *Adv. Mater.* **19,** 2295–2300 (2007).
13. Hoppe, H. & Sariciftci, N. S. Organic solar cells: An overview. *J. Mater. Res.* **19,** 1924–1945 (2004).
14. Winder, C. & Sariciftci, N. S. Low bandgap polymers for photon harvesting in bulk heterojunction solar cells. *J. Mater. Chem.* **14,** 1077–1086 (2004).
15. Hayakawa, A., Yoshikawa, O., Fujieda, T., Uehara, K. & Yoshikawa, S. High performance polythiophene/fullerene bulk-heterojunction solar cell with a TiO_x hole blocking layer. *Appl. Phys. Lett.* **90,** 163517 (2007).
16. Scharber, M. C. *et al.* Design rules for donors in bulk-heterojunction solar cells—towards 10% energy-conversion efficiency. *Adv. Mater.* **18,** 789–794 (2006).
17. Brabec, C. J., Sariciftci, N. S. & Hummenlen, J. C. Plastic solar cells. *Adv. Mater.* **11,** 15–26 (2001).
18. Brabec, C. J. *et al.* Origin of the open circuit voltage of plastic solar cells. *Adv. Funct. Mater.* **11,** 374–380 (2001).
19. Arbogast, J. W. & Foote, C. S. Photophysical properties of C_{70}. *J. Am. Chem. Soc.* **113,** 8886–8889 (1991).
20. Wienk, M. M. *et al.* Efficient methano[70]fullerene/MDMO-PPV bulk heterojunction photovoltaic cells. *Angew Chem. Int. Ed.* **42,** 3371–3375 (2003).
21. Kim, J. Y. *et al.* New architecture for high-efficiency polymer photovoltaic cells using solution-based titanium oxide as an optical spacer. *Adv. Mater.* **18,** 572–576 (2006).
22. Lee, K. *et al.* Air-stable polymer electronic devices. *Adv. Mater.* **19,** 2445–2449 (2007).
23. Cho, S. *et al.* Multilayer bipolar field-effect transistors. *Appl. Phys. Lett.* **92,** 063505 (2008).
24. Persson, N.-K. & Inganas, O. in *Organic Photovoltaics* Ch. 5 (Taylor & Francis, 2005).
25. Slooff, L. H. *et al.* Determining the internal quantum efficiency of highly efficient polymer solar cells through optical modeling. *Appl. Phys. Lett.* **90,** 1435061 (2007).
26. Mayer, A. C., Scully, S. R., Hardin, B. E., Rowell, M. W. & McGehee, M. D. Polymer-based solar cells. *Mater. Today* **10,** 28–33 (2007).
27. Schilinsky, R., Waldauf, C. & Brabec, C. J. Recombination and loss analysis in polythiophene based bulk heterojunction photodetectors. *Appl. Phys. Lett.* **81,** 3885–3887 (2002).
28. Dennler, G. *et al.* Angle dependence of external and internal quantum efficiencies in bulk-heterojunction organic solar cells. *J. Appl. Phys.* **102,** 0545161 (2006).
29. Vacar, D., Maniloff, E. S., McBranch, D. W. & Heeger, A. J. Charge-transfer range for photoexcitations in conjugated polymer/fullerene bilayers and blends. *Phys. Rev. B* **56,** 4573–4577 (1997).
30. Shaw, P. E., Ruseckas, A. & Samuel, I. D. W. Exciton diffusion measurements in poly(3-hexylthiophene). *Adv. Mater.* **20,** 3516–3520 (2008).
31. Kraabel, B. *et al.* Subpicosecond photoinduced electron transfer from conjugated polymers to functionalized fullerenes. *J. Chem. Phys.* **104,** 4267–4273 (1996).
32. Brabec, C. J. *et al.* Transient photoinduced electron transfer process in conjugated polymer/fullerene bulk heterojunction in real time. *Chem. Phys. Lett.* **340,** 232–236 (2001).
33. Yao, Y. Hou, J., Xu, Z., Li, G. & Yang, Y. Effects of solvent mixtures on the nanoscale phase separation in polymer solar cells. *Adv. Funct. Mater.* **18,** 1783–1789 (2008).
34. Gunes, S., Neugebauer, H. & Sariciftci, N. S. Conjugated polymer-based organic solar cells. *Chem. Rev.* **107,** 1324–1338 (2007).
35. Zhang, F. *et al.* Influence of solvent mixing on the morphology and performance of solar cells based on polyfluorene copolymer/fullerene blends. *Adv. Funct. Mater.* **16,** 667–674 (2006).

36. Hoppe, H. & Sariciftci, N. S. Morphology of polymer/fullerene bulk heterojunction solar cells. *J. Mater. Chem.* **16,** 45–61 (2006).
37. Ma, W., Yang, C. & Heeger, A. J. Spatial Fourier-transform analysis of the morphology of bulk heterojunction materials used in plastic solar cells. *Adv. Mater.* **19,** 1387–1390 (2007).
38. Moon, J. S., Lee, J. K., Cho, S., Byun, J. & Heeger, A. J. Columnlike structure of the cross-sectional morphology of bulk heterojunction materials. *Nano Lett.* **9,** 230–234 (2009).
39. Shrotriya, V. *et al.* Accurate measurement and characterization of organic solar cells. *Adv. Funct. Mater.* **16,** 2016–2023 (2006).
40. Metzdorf, J., Winter, S. & Wittchen, T. Radiometry in photovoltaics: calibration of reference solar cells and evaluation of reference values. *Metrologia* **37,** 573–578 (2000).
41. Lee, J. K. *et al.* Processing additives for improved efficiency from bulk heterojunction solar cells. *J. Am. Chem. Soc.* **130,** 3619–3623 (2008).

Acknowledgements

The research leading to the results reported here was supported by the Air Force Office of Scientific Research, the Department of Energy and by a grant from the US Army CERDC. The TiO_x development work was carried out at the Heeger Center for Advanced Materials (Gwangju Institute of Science and Technology (GIST) and UCSB) with support from under the Global Research Laboratory (GRL) Program sponsored by the Korean Government. The authors thank C. Brabec and R. Gaudiana for advice and encouragement, and for supplying the $PC_{70}BM$. The measurements at NREL were carried out by P. Ciszek and K. Emery. We thank them for their help and cooperation.

Additional information

Supplementary information accompanies this paper at www.nature.com/naturephotonics. The authors declare competing financial interests: details accompany the full-text HTML version of the paper at www.nature.com/naturephotonics. Reprints and permission information is available online at http://npg.nature.com/reprintsandpermissions/.
Correspondence and requests for materials should be addressed to K.L. and A.J.H.